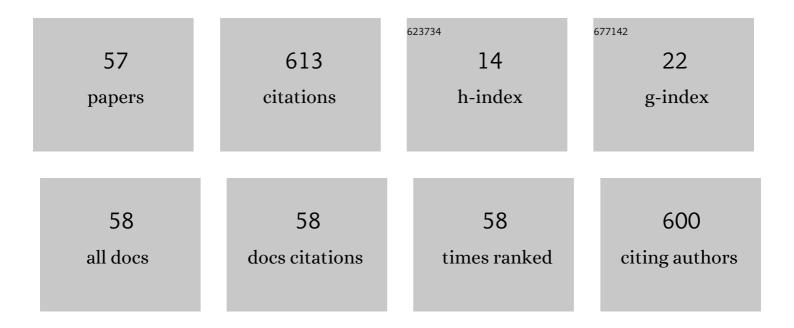
Xiufeng He

List of Publications by Year in descending order

Source: https://exaly.com/author-pdf/4914909/publications.pdf Version: 2024-02-01



YHEENC HE

#	Article	IF	CITATIONS
1	Evaluation and combination of quad-constellation multi-GNSS multipath reflectometry applied to sea level retrieval. Remote Sensing of Environment, 2019, 231, 111229.	11.0	55
2	Deformation Monitoring of Reservoir Dams Using GNSS: An Application to South-to-North Water Diversion Project, China. IEEE Access, 2019, 7, 54981-54992.	4.2	48
3	Water Availability of São Francisco River Basin Based on a Space-Borne Geodetic Sensor. Water (Switzerland), 2016, 8, 213.	2.7	40
4	Estimating Total Discharge in the Yangtze River Basin Using Satellite-Based Observations. Remote Sensing, 2013, 5, 3415-3430.	4.0	36
5	The Influence of Polarimetric Parameters and an Object-Based Approach on Land Cover Classification in Coastal Wetlands. Remote Sensing, 2014, 6, 12575-12592.	4.0	33
6	Analysis and combination of multi-GNSS snow depth retrievals in multipath reflectometry. GPS Solutions, 2020, 24, 1.	4.3	27
7	Gaussian Half-Wavelength Progressive Decomposition Method for Waveform Processing of Airborne Laser Bathymetry. Remote Sensing, 2018, 10, 35.	4.0	24
8	Feasibility of easy-to-implement methods to analyze systematic errors of multipath, differential code bias, and inter-system bias for low-cost receivers. GPS Solutions, 2021, 25, 1.	4.3	23
9	Models, methods and assessment of four-frequency carrier ambiguity resolution for BeiDou-3 observations. GPS Solutions, 2020, 24, 1.	4.3	22
10	Real-time landslide monitoring of Pubugou hydropower resettlement zone using continuous GPS. Natural Hazards, 2013, 69, 1647-1660.	3.4	21
11	Millimeter to centimeter scale precision water-level monitoring using GNSS reflectometry: Application to the South-to-North Water Diversion Project, China. Remote Sensing of Environment, 2021, 265, 112645.	11.0	21
12	MEMS IMU and two-antenna GPS integration navigation system using interval adaptive Kalman filter. IEEE Aerospace and Electronic Systems Magazine, 2013, 28, 22-28.	1.3	19
13	Study on the Quality Control for Periodogram in the Determination of Water Level Using the GNSS-IR Technique. Sensors, 2019, 19, 4524.	3.8	19
14	Scattering Feature Set Optimization and Polarimetric SAR Classification Using Object-Oriented RF-SFS Algorithm in Coastal Wetlands. Remote Sensing, 2020, 12, 407.	4.0	16
15	Ocean Wave Separation Using CEEMD-Wavelet in GPS Wave Measurement. Sensors, 2015, 15, 19416-19428.	3.8	14
16	Integration of InSAR and GPS for hydraulic engineering. Science in China Series D: Earth Sciences, 2007, 50, 111-124.	0.9	13
17	Improving Short Term Clock Prediction for BDS-2 Real-Time Precise Point Positioning. Sensors, 2019, 19, 2762.	3.8	10
18	Snow Depth Estimation on Slopes Using GPS-Interferometric Reflectometry. Sensors, 2019, 19, 4994.	3.8	10

XIUFENG HE

#	Article	IF	CITATIONS
19	Classification of coastal wetlands in eastern China using polarimetric SAR data. Arabian Journal of Geosciences, 2015, 8, 10203-10211.	1.3	9
20	Improving Clock Prediction Algorithm for BDS-2/3 Satellites Based on LS-SVM Method. Remote Sensing, 2019, 11, 2554.	4.0	9
21	Terrain Point Cloud Assisted GB-InSAR Slope and Pavement Deformation Differentiate Method in an Open-Pit Mine. Sensors, 2020, 20, 2337.	3.8	9
22	An Assessment of Recently Released High-Degree Global Geopotential Models Based on Heterogeneous Geodetic and Ocean Data. Frontiers in Earth Science, 2021, 9, .	1.8	9
23	Distributed Orbit Determination for Global Navigation Satellite System with Inter-Satellite Link. Sensors, 2019, 19, 1031.	3.8	8
24	Coherent superposition of multi-GNSS wavelet analysis periodogram for sea-level retrieval in GNSS multipath reflectometry. Advances in Space Research, 2020, 65, 1781-1788.	2.6	8
25	Study on the Exploration of Spaceborne GNSS-R Raw Data Focusing on Altimetry. IEEE Journal of Selected Topics in Applied Earth Observations and Remote Sensing, 2020, 13, 6142-6154.	4.9	8
26	Real-Time Cycle Slip Detection and Repair Method for BDS-3 Five-Frequency Data. IEEE Access, 2021, 9, 51189-51201.	4.2	8
27	A Correction Method of Height Variation Error Based on One SNR Arc Applied in GNSS–IR Sea-Level Retrieval. Remote Sensing, 2022, 14, 11.	4.0	8
28	Effect of Cloud Fraction on Arctic Low-Level Temperature Inversions in AIRS Observations Over Both Land and Ocean. IEEE Transactions on Geoscience and Remote Sensing, 2018, 56, 2025-2032.	6.3	7
29	Refinement of Mean Dynamic Topography Over Island Areas Using Airborne Gravimetry and Satellite Altimetry Data in the Northwestern South China Sea. Journal of Geophysical Research: Solid Earth, 2021, 126, e2021JB021805.	3.4	6
30	Local Enhancement of Marine Gravity Field over the Spratly Islands by Combining Satellite SAR Altimeter-Derived Gravity Data. Remote Sensing, 2022, 14, 474.	4.0	6
31	A wavelet domain detail compensation filtering technique for InSAR interferograms. International Journal of Remote Sensing, 2011, 32, 7985-7995.	2.9	5
32	Validation of 7 Years in-Flight HY-2A Calibration Microwave Radiometer Products Using Numerical Weather Model and Radiosondes. Remote Sensing, 2019, 11, 1616.	4.0	5
33	The parameterization of mean dynamic topography based on the Lagrange basis functions. Advances in Space Research, 2020, 66, 2122-2140.	2.6	5
34	Calibrating the Haiyang-2A Calibration Microwave Radiometer When the 18.7-GHz Band Fails. IEEE Transactions on Geoscience and Remote Sensing, 2022, 60, 1-10.	6.3	5
35	Vertical and horizontal displacements of a reservoir slope due to slope aging effect, rainfall, and reservoir water. Geodesy and Geodynamics, 2021, 12, 266-278.	2.2	5
36	Rapid calibration of HY-2A satellite-borne microwave radiometer using coastal GNSS observations. Journal of Geodesy, 2022, 96, 1.	3.6	5

XIUFENG HE

#	Article	IF	CITATIONS
37	Effects and disturbances on GPS-derived zenith tropospheric delay during the CONT08 campaign. Advances in Space Research, 2012, 50, 632-641.	2.6	4
38	Application of Gaofen-6 Images in the Downscaling of Land Surface Temperatures. Remote Sensing, 2022, 14, 2307.	4.0	4
39	An improved PolSAR image speckle reduction algorithm based on LMMSE and RICA. Modern Physics Letters B, 2017, 31, 1740033.	1.9	3
40	The Application of Robust Least Squares Method in Frequency Lock Loop Fusion for Global Navigation Satellite System Receivers. Sensors, 2020, 20, 1224.	3.8	3
41	Mean Dynamic Topography Modeling Based on Optimal Interpolation from Satellite Gravimetry and Altimetry Data. Applied Sciences (Switzerland), 2021, 11, 5286.	2.5	3
42	Investigation on Geometry Computation of Spaceborne GNSS-R Altimetry over Topography: Modeling and Validation. Remote Sensing, 2022, 14, 2105.	4.0	3
43	Quality assessment of ZiYuan-3 multispectral and panchromatic images fusion: applied in Jiangsu coastal wetland area, China. Journal of Applied Remote Sensing, 2015, 9, 095089.	1.3	2
44	A novel partitioned matrixâ€based parameter update method embedded in variational Bayesian for underwater positioning. IET Control Theory and Applications, 2022, 16, 414-428.	2.1	2
45	Coastal Mean Dynamic Topography Recovery Based on Multivariate Objective Analysis by Combining Data from Synthetic Aperture Radar Altimeter. Remote Sensing, 2022, 14, 240.	4.0	2
46	Rock mass structural surface trace extraction based on transfer learning. Open Geosciences, 2022, 14, 98-110.	1.7	2
47	Analysis on the optimal system parameters of space-borne SAR for urban areas extraction. Optik, 2015, 126, 1236-1239.	2.9	1
48	Collision Probability Prediction and Orbit Maneuvering Probability Determination of Non-Cooperative Space Object Orbit. Remote Sensing, 2020, 12, 3310.	4.0	1
49	Development of an Imagewise Stacking Method to Mitigate Atmospheric Effect With an Application to Lianyan Railway. IEEE Journal of Selected Topics in Applied Earth Observations and Remote Sensing, 2021, 14, 4787-4797.	4.9	1
50	Comparison of the Segmentation Results of Two Carrier Tracking Loop Types and Analysis of Theoretical Influencing Factors. Remote Sensing, 2021, 13, 2035.	4.0	1
51	Rock mass structure surface extraction method using multiview images based on integration of multimodal semantic features and a full convolution neural network model. Journal of Applied Remote Sensing, 2022, 16, .	1.3	1
52	Sea Surface States Detection in Polar Regions Using Measurements of Ground-Based GNSS Interferometric Reflectometry. IEEE Transactions on Geoscience and Remote Sensing, 2022, 60, 1-14.	6.3	1
53	Spectrally Consistent Mean Dynamic Topography by Combining Mean Sea Surface and Global Geopotential Model Through a Least Squares-Based Approach. Frontiers in Earth Science, 2022, 10, .	1.8	1
54	A Proposed Algorithm to Compute the Stress-Strain Plastic Region and Displacement of a Deep-Lying Tunnel Considering Intermediate Stress and Strain-Softening Behavior. Applied Sciences (Switzerland), 2022, 12, 85.	2.5	1

XIUFENG HE

#	Article	IF	CITATIONS
55	An Orbital Error Correction Model Based on Triplet Network and Shrunken Estimation. IEEE Geoscience and Remote Sensing Letters, 2022, 19, 1-5.	3.1	1
56	Monitoring land subsidence using interferometric synthetic aperture radar time-series analysis: a case of Shanghai Pilot Free Trade Zone. Journal of Applied Remote Sensing, 2022, 16, .	1.3	0
57	Numerical solution for circular tunnel excavated in strain-softening rock masses considering damaged zone. Scientific Reports, 2022, 12, 4465.	3.3	0